A Hybrid Winding Design to Reduce AC Losses in Electrical Machines with Bar Conductors

Wenjun Zhu, *Graduate Student Member, IEEE*, Yangyu Sun, Xiao Chen, *Senior Member, IEEE*, and Geraint W. Jewell

***Abstract*—Bar conductor windings with rectangular cross-sections are increasingly used in electrical vehicle traction applications for their high slot fill factor, reduced losses, improved heat transfer, and manufacturing repeatability. However, AC losses from eddy currents due to skin and proximity effects limit their performance at high frequencies. This paper proposes a hybrid winding design to reduce AC losses in electrical machines with bar conductors. The design integrates copper conductors with outer layers of low-conductivity materials, such as aluminium or brass, to leverage the low DC resistance of copper and mitigate AC losses caused by skin and proximity effects at high frequencies. A comprehensive analytical model and finite element analysis are developed to optimize and validate the design, supported by experimental results from brass-copper hybrid conductors. The proposed design reduces winding losses without altering the original winding layout, providing a practical and efficient solution for enhancing the performance of traction machines.**

***Index Terms*— AC losses, bar conductor, proximity effect, skin effect.**

I. INTRODUCTION

BAR conductor windings have become an increasingly popular solution for electric vehicle (EV) traction machines, with automated manufacturing processes continually improving. The major advantage of using bar conductors is the high slot fill factor, resulting in reduced winding loss compared to wound windings with circular conductors. Despite the existence of different configurations of bar conductors, such as hairpin windings, form-wound concentrated winding, lap, or diamond winding, they all share one common principle, viz., utilizing rectangle-shaped cross-section conductors to fit into parallel slots, thereby maximizing the slot fill factor.

High efficiency is one desirable attribute for electrical machines in EV applications. Whereas the low DC resistance or DC loss of bar conductors is well recognized [1], their adoption is often hindered by concerns over AC losses [2, 3]. It is essential for the machine to function effectively across a wide speed range in EV applications. However, the AC losses increase with the square of the rotational speed for bar conductors due to their relatively larger cross-sectional area.

Commercially available EV/HEV traction machines often feature 6 poles (e.g., Tesla Model 3), 8 poles (e.g., Toyota Prius), or 12 poles (e.g., BMW i3), and have a speed range of 12,000-20,000 rpm. Hence, the fundamental frequency range encountered in commercial machines are usually up to 2000 Hz. Higher speed ranges around 30,000 rpm are emerging in the automotive industry [4]. And this trend toward higher speed of EV traction machines, will further exacerbate the challenges of managing AC loss in conductors. At higher speeds, the skin effect and proximity effect become more pronounced, leading to increased eddy current losses in the winding conductors.

Several concepts have been proposed in the literature to address this issue. One such concept is the asymmetric winding, where small bars are positioned close to the slot opening, while larger cross-section bars are placed near the slot bottom. This approach was proposed and validated through Finite Element Analysis (FEA) in [5]. Windings with shaped cross-sections were proposed in [6]. This approach aligned trapezoidal conductor geometries with the flux lines in the slot, such that the additional proximity effect is minimized. Pentagonal shaped conductors placed close to stator opening were proposed in [7] to reduce AC losses in permanent magnet synchronous machines.

Additionally, increasing the number of conductors [8], and implementing a segmented hairpin topology in the radial direction [9-11] and/or in the circumferential direction [12, 13], have also shown promise in reducing AC losses. However, these methods are constrained by their manufacturing complexity [10]. Increasing the number of conductor divisions results in a higher proportion of insulating coating on the conductor. Consequently, excessive division reduces the cross-sectional area of the conductor, potentially leading to an elevation in copper loss due to heightened conductor resistance [12]. Segmented hairpin topologies typically necessitate thinner conductors while maintaining constant width, posing insulation challenges, especially with a higher width-to-thickness ratio.

Another approach is to adopt a hybrid winding, which involves incorporating stranded conductors or Litz wire at the slot opening [14] or replacing the copper conductors with aluminium [15, 16]. This method leverages the advantages of both types of conductors to reduce the overall loss. Nevertheless, all of these concepts require a complex design of the winding layout and meticulous transposition of conductors

Wenjun Zhu is with the University of Sheffield, Sheffield, S10 4DE, UK (e-mail: wzhu24@ sheffield.ac.uk).

Yangyu Sun is with the University of Sheffield, Sheffield, S10 4DE, UK (e-mail: ysun78@sheffield.ac.uk).

Xiao Chen is with the University of Sheffield, Sheffield, S10 4DE, UK (e-mail: xiao.chen@sheffield.ac.uk).

Geraint W. Jewell is with the University of Sheffield, Sheffield, S10 2TN, UK (e-mail: g.jewell@sheffield.ac.uk).

between slots [17]. Furthermore, aluminium windings with a high slot fill factor of 83.8% have been employed to balance DC loss, resulting in reduced AC losses and machine weight compared to copper windings [18].

While extensive research has been conducted on mitigating AC losses and optimizing motor performance under high-speed conditions, current solutions, such as using more layers of conductors, often fail to effectively balance manufacturability, cost, and loss reduction. This research gap underscores the need for innovative conductor designs and analytical models tailored specifically to high-speed applications to minimize AC losses while maintaining practical manufacturing considerations.

Progress in metal additive manufacturing enables the creation of intricate three-dimensional structures using copper, while developments in powder metallurgy and higher laser powers allow for the printing of copper with electrical conductivity approaching 100% IACS. Utilizing complex three-dimensional printed Litz windings has proven effective for comparing and benchmarking designs against solid conductor and Type 8 Litz alternatives [19, 20]. An asymmetrical winding configuration was made through additive manufacturing with AlSi10Mg to minimize winding loss [21]. Additionally, conductors featuring a Hilbert-cross section pattern, enabled by additive manufacturing, demonstrated a loss reduction by approximately 25% compared to square-cross section conductors at high frequencies [22].

In addition to offering unrivalled geometric flexibility, additive manufacturing also has the potential to achieve engineered material electrical properties through precise process control. In [23], researchers explore the performance advantages of functionally grading electrical conductivity to effectively balance DC and AC winding loss components. They demonstrated the practical feasibility of manufacturing such windings and showcased the achievable range of electrical conductivity for CuCrZr. In [24], the implementation of varying electrical conductivity across different conductor layers with AlSi10Mg was demonstrated to minimize AC loss.

The idea of combining aluminium and copper conductors has been investigated in [25] for circular wires at a frequency of 60 Hz for both aluminium conductors with copper cores and copper conductors with aluminium cores.

In this paper, copper bar conductors with an outer layer of low electrical conductivity materials (e.g., aluminium, brass) are proposed to maximize the advantages of the low DC resistance of copper and the lower AC resistance of aluminium. By appropriately selecting the thickness of the outer aluminium layer, it becomes possible to reduce overall winding losses over a driving cycle while maintaining a realistic conductor manufacturing route in which the coil forming process is unmodified from a traditional copper bar winding. The hybrid arrangement of metallic materials in the conductor level allows the physical configuration of the original design of winding layouts to remain unchanged.

II. Proposed concept

AC currents in windings induce eddy currents in conductors, which, at high frequencies, lead to significant skin and proximity effects, generating additional Joule loss, referred to AC loss. The total winding loss, P_{tot}, is the sum of DC loss (P_{DC}) and AC loss (P_{AC}), as expressed in (1). Alternatively, it can be calculated using the AC resistance (R_{AC}), as shown in (2).

$$P_{tot} = P_{DC} + P_{AC} \quad (1)$$

$$P_{tot} = I^2 R_{AC} \quad (2)$$

As presented in (3) and (4), for a material of electrical conductivity σ, the DC loss is inversely proportional to σ but the AC loss would be proportional to σ (providing the frequency is such that the reaction field of eddy currents can be neglected) [26].

$$P_{DC} \propto 1/\sigma \quad (3)$$

$$P_{AC} \propto \sigma \quad (4)$$

This leads to a trade-off between the DC loss and the AC loss in windings to minimize the total winding loss. In the general case, then for a given geometry and configuration, an aluminium winding will exhibit less total winding loss compared to the copper winding once the frequency is above a certain threshold. This is due to aluminium having a lower electrical conductivity, resulting in lower AC losses.

Both skin effect and proximity effect tend to concentrate the net current towards the outer surface of a conductor. By placing a layer of lower conductivity material (e.g., aluminium) on the outside with copper in the centre, it is possible to modify the distribution of current flow across the conductor and leverage some benefits of both materials. In the DC to low frequency range, the high electrical conductivity of copper at the centre causes more currents to flow through it. However, as the frequency increases to the medium to high range, more current tend to flow in the outer layer of low conductivity material. In this frequency range, the hybrid metal conductor behaves in a manner similar to an aluminium conductor, resulting in lower AC losses and overall total losses.

For the initial study, a single slot model with 8 series connected conductors was investigated by finite element analysis using the Altair Flux software suite. The windings are assumed to be operating at a uniform working temperature of 100°C. For comparison purposes, the pure copper winding (Scheme A) is taken as the baseline as shown in Fig. 1 (a). One embodiment of the proposed hybrid winding concept is depicted in Fig. 1 (b). This is denoted as Scheme B and consists of 3-layer sandwich-type conductors making up each of the 8 series turns with rectangular aluminium layers in the upper and lower regions and copper layer in the middle. It is a well-recognized consequence of Ampere's Law that the conductors closer to the slot opening experience higher leakage flux, and hence higher AC losses than conductors near the slot bottom. To address this issue, along the depth of the slot, the thickness of aluminium layers is varied between successive turns to achieve a reduction in the total winding loss. The total conductor fill factor remains the same as that in the baseline copper winding.

However, Scheme B would introducing a high variety of component parts into the manufacturing process as the thickness of aluminium layers varies from turns to turns. It would require significant performance benefits to offset the cost and complexity and would inevitably be influenced by the production volume.

Furthermore, such an approach would require a mechanically robust and electrically sound welding process for these dual metal connections with welding parameters varying between different conductor compositions. An alternative approach is to divide the conductors into two groups as Scheme C in Fig. 1 (c). It consists of 4 copper conductors and 4 hybrid conductors with the same cross-section configuration.

The conductors are designated as T1 to T8 from the slot bottom to slot opening as shown in Fig. 1. This figure represents a single slot without depicting the rotor. Key parameters of the single slot model are defined in Table 1.

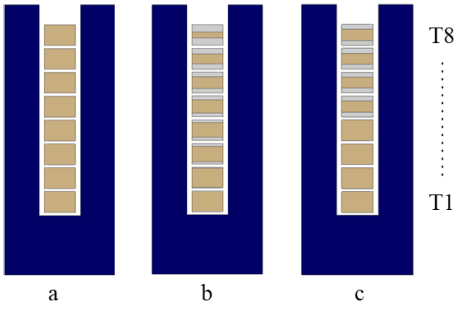

Fig. 1. Single slot model with 8 conductors. (a) Scheme A: pure copper conductors; (b) Scheme B: hybrid 3-layer conductors with non-uniform layer thickness of each turn; (c) Scheme C: 4 copper conductors and 4 hybrid conductors with uniform layer thickness.

TABLE 1. KEY PARAMETERS OF SINGLE SLOT MODEL

Parameters	Value
Slot width	4.15 mm
Slot depth	21.2 mm
Conductor width	3.12 mm
Conductor height	2.10 mm
Slot fill factor	60%
Core stack length	61 mm
Copper electrical conductivity at 100°C	4.48×10^7 S/m
Aluminium electrical conductivity at 100°C	2.70×10^7 S/m
DC resistance of copper winding (active region only) R_{DC-Cu}	1.66 mΩ

It is important to recognize that two-dimensional consideration of current flow in such conductors would be unaffected by the presence or otherwise of an insulating layer between the aluminium and copper regions, since the only component of current is along the length of the conductor, i.e. in the z-direction of a cartesian coordinate system if the two-dimensional cross-section is laid out in the x-y plane. Hence, the two-dimensional analytical and finite element analysis presented in this paper is equally applicable to insulated and non-insulated cases within the cross-section of a single turn. In practice, the different behaviour that would be encountered in the end-windings, where the degree of current redistribution will inevitable be lower, is likely to result in some current flow between the aluminium and copper regions near the ends of the stator core and hence some difference in behaviour between insulated and non-insulated cases.

It is important to note that for non-insulated cases, more repeatable performance, particularly in terms of avoiding localized hot spots, is likely to be achieved if the conductors are metallurgically bonded to each other using a method that results in a continuous low resistance interface rather than having non-insulated aluminium and copper conductors simply bound together by an insulating over-wrap and hence in spatially intermittent contact. In the case where the separately insulated copper and aluminium conductors are used, i.e. the winding is formed by parallel bars of otherwise standard insulated copper and aluminium rectangular conductors, the only impact on the analysis presented in this paper is the effective packing factor rather than electrical behaviour per se.

A first estimate of the proportions of each conductor which is allocated to copper and aluminium to optimize the loss was achieved by sweeping the thickness of the aluminium layer at an overall current of 80A RMS (equivalent to 12.21A/mm^2 RMS), The net magneto-motive force in the slot remains constant and hence the torque remains fixed.

Table 2 lists the optimal thickness of aluminium layers for each turn established using this method, which yields the minimum total winding loss at fundamental excitation frequencies of 500 Hz. The total winding loss and comparison with the pure copper windings are presented in Table 3.

TABLE 2. OPTIMAL THICKNESS OF EACH TURN AT 500 HZ

Conductor index	Thickness of aluminium layer – Scheme B	Thickness of aluminium layer – Scheme C
T1	0 mm (copper only)	0 mm (copper only)
T2	0 mm (copper only)	0 mm (copper only)
T3	0 mm (copper only)	0 mm (copper only)
T4	0.01 mm	0 mm (copper only)
T5	0.18 mm	0.36 mm
T6	0.31 mm	0.36 mm
T7	0.40 mm	0.36 mm
T8	0.46 mm	0.36 mm

TABLE 3. TOTAL WINDING LOSS REDUCTION

Frequency	Scheme A	Scheme B	Scheme C
500 Hz	17.01 W	16.22W (-4.64%)	16.27 W (-4.35%))
1000 Hz	35.83 W	30.41W (-15.13%)	30.49 W (-14.90%))
1500 Hz	66.27 W	53.62 W (-19.09%)	53.73 W (-18.92%)
2000 Hz	107.06 W	85.21 W (-20.41%)	85.36 W (-20.27%)

Although Scheme B can provide the greatest reduction in winding losses, they would considerably complicate the manufacturing process for continuous bar windings, as the cross-sectional composition would need to vary between successive turns. This arrangement is more feasible with a hairpin winding, where each turn is a separate conductor that is joined to adjacent turns in the coil by in-situ welding [4].

In contrast, Scheme C represents a practical solution that strikes a balance between performance, manufacturability, and cost-

efficiency. The main reason for selecting this configuration is to minimize variations in conductor structure during manufacturing, thus reducing costs. While this design may not achieve the best possible reduction in AC losses, it is a viable solution for actual applications.

The AC loss in the end-windings is modest compared to the AC loss in the active regions of windings in the stator slots due to the fact that the magnetic field in the end-winding region is much weaker. Hence in principle at least, it is possible to have the hybrid conductor cross-section in the active winding region and copper only conductor for the end-windings, as shown in Fig. 2. Then this design would still bring the majority of the total losses reduction but would ensure that the in-situ welding process for the hairpin connection would occur in a copper only conductor. This would make the joining process for successive turns the same as existing industrial process and avoids the challenges posed by connecting bi-material conductors. Such a topology would still require a high integrity and low electrical resistance connection at the ends of the aluminium regions. However, this would be done ex-situ in terms of the stator and prior to the application of the insulation coating and hence a number of joining methods and subsequent post joining processes could be used to ensure a high integrity joint. Further discussion on material selection and manufacturing processes can be found in Section V.

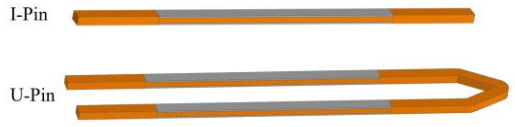

Fig. 2. Proposed I-Pin and U-Pin conductors.

III. Analysis of Hybrid 3-Layered Winding

This section presents an analytical framework for understanding and optimizing hybrid 3-layered windings which is validated through comparisons with FEA results. This analytical approach is deployed to explore the influence of layer thickness on performance characteristics.

A. Analytical Modelling

An analytical method for calculating the AC resistance of conventional single material rectangular conductors is presented in [27]. Here, we present an analytical model of hybrid 3-layered conductors. As shown in Fig. 3, there are N conductors numbered sequentially from the slot bottom. The slot width is denoted as b. The origin of the cartesian coordinate system is set at the centre of slot bottom as shown. The permeability of stator core is assumed to be infinite. The magnetic field strength, $\boldsymbol{H}$, is assumed to follow the simplified loops (denoted by dashed lines) which are assumed to be normal to the slot wall.

The p-th conductor in the winding is shown in Fig. 3 and is of width c and height h. The central copper region is sandwiched between conductor is made up of two layers of aluminium which are individually assumed to be of equal thickness h_1. The position of the bottom edge, the upper edge and the boundaries between the copper layer and aluminium layers are denoted as y_1, y_2, y_3, and y_4 respectively. The aluminium electrical conductivity is σ_1 while that of the copper is σ_2 is. The magnetic permeability of copper and aluminium are assumed to be μ_0. The gaps between the adjacent conductors which make up one turn are neglected.

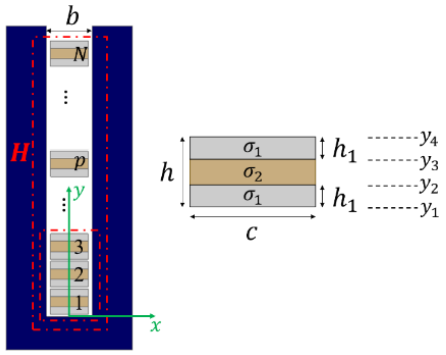

Fig. 3. Single slot model with 3-layered conductors and the p-th conductor.

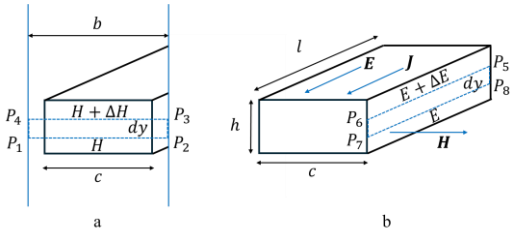

Fig. 4. The magnetic field and electric field inside the conductor.

Considering a closed loop $P_1P_2P_3P_4$ as shown in Fig. 4 (a), then applying the Ampere's Law around this loop yields:

$$\boldsymbol{H}b - (\boldsymbol{H} + \Delta\boldsymbol{H})b = \boldsymbol{J}cdy \tag{5}$$

$$\boldsymbol{H}b - \left(\boldsymbol{H} + \frac{\partial \boldsymbol{H}}{\partial y}dy\right)b = \sigma(y)\boldsymbol{E}cdy \tag{6}$$

$$-\frac{\partial \boldsymbol{H}}{\partial y} = \frac{c}{b}\sigma(y)\boldsymbol{E} \tag{7}$$

where $\sigma(y)$ is a piecewise function of y:

$$\sigma(y) = \begin{cases} \sigma_1 \ (y_1 \le y < y_2) \\ \sigma_2 \ (y_2 \le y \le y_3) \\ \sigma_1 \ (y_3 < y \le y_4) \end{cases} \tag{8}$$

Considering a closed loop $P_5P_6P_7P_8$ as shown in Fig. 4 (b), then applying the Faraday's Law yields:

$$(\boldsymbol{E} + \Delta\boldsymbol{E})l - \boldsymbol{E}l = -\frac{d\boldsymbol{\phi}}{dt} \tag{9}$$

$$\left(\boldsymbol{E} + \frac{\partial \boldsymbol{E}}{\partial y}dy\right)l - \boldsymbol{E}l = -\frac{d}{dt}(\mu_0 \boldsymbol{H}ldy) \tag{10}$$

$$-\frac{\partial \boldsymbol{E}}{\partial y} = \mu_0 \frac{\partial \boldsymbol{H}}{\partial t} \tag{11}$$

Taking the partial derivative of (7) with respect to y, and then solving it together with (11), yields:

$$\frac{\partial^2 \boldsymbol{H}}{\partial y^2} = \frac{c}{b}\mu_0 \sigma(y)\frac{\partial \boldsymbol{H}}{\partial t} \tag{12}$$

This is the one-dimensional form of the standard eddy current equation. If the excitation is a sinusoidal current with angular frequency ω, then this governing eddy current equation can be solved in the complex domain.

$$\boldsymbol{H}=\begin{cases}C_1e^{-\gamma_1 y}+C_2e^{\gamma_1 y}\ (y_1\le y\le y_2)\\ C_3e^{-\gamma_2 y}+C_4e^{\gamma_2 y}\ (y_2\le y\le y_3)\\ C_5e^{-\gamma_1 y}+C_6e^{\gamma_1 y}\ (y_3\le y\le y_4)\end{cases} \tag{13}$$

where γ_1, γ_2, α_1 and α_2 are listed in (14).

$$\begin{cases}\gamma_1=\sqrt{j\frac{c}{b}\omega\mu_0\sigma_1}=\alpha_1+j\beta_1\\ \gamma_2=\sqrt{j\frac{c}{b}\omega\mu_0\sigma_2}=\alpha_2+j\beta_2\\ \alpha_1=\beta_1=\sqrt{\frac{c\omega\mu_0\sigma_1}{2b}}\\ \alpha_2=\beta_2=\sqrt{\frac{c\omega\mu_0\sigma_2}{2b}}\end{cases} \tag{14}$$

The boundary conditions are:

At $y_1=(p-1)h$:

$$\boldsymbol{H}_1=\frac{(p-1)\boldsymbol{I_m}}{b} \tag{15}$$

At $y_4=ph$:

$$\boldsymbol{H}_4=\frac{p\boldsymbol{I_m}}{b} \tag{16}$$

At $y_2=(p-1)h+h_1$:

$$\begin{aligned}\boldsymbol{H}_2&=C_1e^{-\gamma_1 y_2}+C_2e^{\gamma_1 y_2}\\ &=C_3e^{-\gamma_2 y_2}+C_4e^{\gamma_2 y_2}\end{aligned} \tag{17}$$

$$\begin{aligned}\boldsymbol{E}_2&=-\frac{b}{c\sigma_1}(-\gamma_1C_1e^{-\gamma_1 y_2}+\gamma_1C_2e^{\gamma_1 y_2})\\ &=-\frac{b}{c\sigma_2}(-\gamma_2C_3e^{-\gamma_2 y_2}+\gamma_2C_4e^{\gamma_2 y_2})\end{aligned} \tag{18}$$

At $y_3=ph-h_1$:

$$\begin{aligned}\boldsymbol{H}_3&=C_5e^{-\gamma_1 y_3}+C_6e^{\gamma_1 y_3}\\ &=C_3e^{-\gamma_2 y_3}+C_4e^{\gamma_2 y_3}\end{aligned} \tag{19}$$

$$\begin{aligned}\boldsymbol{E}_3&=-\frac{b}{c\sigma_1}(-\gamma_1C_5e^{-\gamma_1 y_3}+\gamma_1C_6e^{\gamma_1 y_3})\\ &=-\frac{b}{c\sigma_2}(-\gamma_2C_3e^{-\gamma_2 y_3}+\gamma_2C_4e^{\gamma_2 y_3})\end{aligned} \tag{20}$$

Then C_1-C_6 can be established by solving (13-20). Once C_1-C_6 are obtained, Equation (13) can be used to calculate the magnetic field $\boldsymbol{H}$. By multiplying with permeability μ_0, the flux density can be obtained as:

$$\boldsymbol{B}=\begin{cases}\mu_0C_1e^{-\gamma_1 y}+\mu_0C_2e^{\gamma_1 y}\ (y_1\le y\le y_2)\\ \mu_0C_3e^{-\gamma_2 y}+\mu_0C_4e^{\gamma_2 y}\ (y_2\le y\le y_3)\\ \mu_0C_5e^{-\gamma_1 y}+\mu_0C_6e^{\gamma_1 y}\ (y_3\le y\le y_4)\end{cases} \tag{21}$$

From (7), the electric field strength can be expressed as:

$$\boldsymbol{E}=-\frac{b}{c\sigma(y)}\frac{\partial\boldsymbol{H}}{\partial y} \tag{22}$$

Substituting (13) into (22) yields:

$$\boldsymbol{E}=\begin{cases}-\frac{b}{c\sigma_1}\frac{\partial}{\partial y}(C_1e^{-\gamma_1 y}+C_2e^{\gamma_1 y})\ (y_1\le y\le y_2)\\ -\frac{b}{c\sigma_2}\frac{\partial}{\partial y}(C_3e^{-\gamma_2 y}+C_4e^{\gamma_2 y})\ (y_2\le y\le y_3)\\ -\frac{b}{c\sigma_1}\frac{\partial}{\partial y}(C_5e^{-\gamma_1 y}+C_6e^{\gamma_1 y})\ (y_3\le y\le y_4)\end{cases} \tag{23}$$

Hence, the current density can be derived from (23) by simply multiplying by the electrical conductivity:

$$\boldsymbol{J_m}=\begin{cases}-\frac{b}{c}(-\gamma_1C_1e^{-\gamma_1 y}+\gamma_1C_2e^{\gamma_1 y})\ (y_1\le y\le y_2)\\ -\frac{b}{c}(-\gamma_2C_3e^{-\gamma_2 y}+\gamma_2C_4e^{\gamma_2 y})\ (y_2\le y\le y_3)\\ -\frac{b}{c}(-\gamma_1C_5e^{-\gamma_1 y}+\gamma_1C_6e^{\gamma_1 y})\ (y_3\le y\le y_4)\end{cases} \tag{24}$$

It can be observed from (24) that, as would be expected, the current densities at different values of y are not in phase.

The active power consumed in the first aluminium layer can be calculated as:

$$P_{L1}=\int_{y_1}^{y_2}|\boldsymbol{J_m}|^2\frac{1}{2\sigma_1}cldy=\int_{y_1}^{y_2}\boldsymbol{J_m}\cdot\boldsymbol{J_m}^*\frac{1}{2\sigma_1}cldy \tag{25}$$

In a similar manner to P_{L1}, the active power consumed in the second copper layer and the third aluminium layer P_{L2} and P_{L3} can be derived from the volume integral of the square of the current density. Hence, the total losses in the p-th conductor would be the sum of P_{L1}, P_{L2} and P_{L3}:

$$P_p=P_{L1}+P_{L2}+P_{L3} \tag{26}$$

By sweeping p from 1 to N to account for all the conductors in the slot, the total winding losses of the slot can be expressed as:

$$P=\sum_{p=1}^{N}P_p \tag{27}$$

In summary, the total winding losses can be analytically calculated as a function of layer thickness h_1, angular frequency ω, and the amplitude of the excitation current I_m, subject to that the other geometry information such as the slot width, the conductor width and the conductor height are determined.

$$P=f(h_1,\omega,I_m) \tag{28}$$

For a single working point, i.e. a given combination of ω_0 and I_{m0},the optimized layer thickness to minimize the total winding losses would h_1 satisfied when:

$$\frac{dP}{dh_1}=\frac{df(h_1,\omega_0,I_{m0})}{dh_1}=0 \tag{29}$$

This optimization can be extended to a complete driving cycle which consists of k working points (ω_1,I_{m1}), (ω_2,I_{m2}), …(ω_k,I_{mk}), and corresponding time durations of each working points are t_1, t_2,… t_k. In such a case, the energy consumption over the driving cycle is:

$$W=\sum_{i=1}^{k}P_it_i=\sum_{i=1}^{k}f(h_1,\omega_i,I_{mi})t_i \tag{30}$$

The optimized layer thickness is achieved when:

$$\frac{dW}{dh_1}=0 \tag{31}$$

Another more straightforward and pragmatic means to arrive at a useful working approximation to the optimal thickness would be sweeping h_1 from 0 to $h/2$ at a step size of the manufacture tolerance. In this research, 0.01mm is taken as the minimum step size. As this analytical model calculated the losses of each conductor in turn, it is also suitable for the non-uniform 3-layered winding, which can lead to different thickness of outer layers for different conductors.

B. FEA Validation

For the same single slot model presented previously in Fig. 1 (c), the analytical calculation results and those from FEA can be compared. For the case of h_1=0.36 mm, the current density distribution is shown in Fig. 5 at 500 Hz alongside a zoomed-in view of the 3 turns nearest the slot opening (T5-T8).

By setting the electrical conductivity $\sigma_1=\sigma_2=4.48\times10^7$ S/m, the analytical model represents the simple case of a copper only winding.

The variation in the peak current density distribution within each conductor in the y direction of the hybrid 3-layered winding is shown in Fig. 6 for both the analytical calculation and the FEA model at 500 Hz. Fig. 7 shows the magnitude of the current density distribution of each conductor in the y direction of the Scheme C and Scheme A. At low frequencies

(e.g. 50 Hz), the skin and proximity effects are insignificant, so the current density distribution primarily depends on the material conductivity. This results in flat current density profiles in pure copper conductors and a stepped profile in hybrid conductors. As the frequency increases to 500 Hz and 1000 Hz, the skin and proximity effects cause the current to concentrate on the upper and lower surfaces of the pure copper conductors. This phenomenon is more pronounced in the conductors close to the slot opening than that in the conductors close to the slot bottom. In the case of hybrid conductors, the highest current density is observed at the boundary edge of the middle copper layer, but with a reduced peak value compared to pure copper conductors. For example, the peak value of current density in T8 at 1000 Hz has been reduced from ~80 A/mm^2 to ~55 A/mm^2. It should be noted that only the magnitude of current density is reflected in Fig. 6 and Fig. 7. Moreover, these current densities are not in the same phase, the overall averaged current density of each conductor is still 12.21 A/mm^2 RMS. The analytical predictions of current density agree well with the FEA predictions over the frequency range of interest. By way of example, the maximum current density in T8 is 32.27 A/mm^2 predicted by FEA and 32.55 A/mm^2 predicted by the analytical calculation, an error of less than 1%. One reason why the analytical calculated current density is slightly higher than the FEA results can be explained by the assumption that the core permeability is infinite in the analytical model, which in turn leads to overestimation of $\boldsymbol{H}$, and hence overestimation on current density.

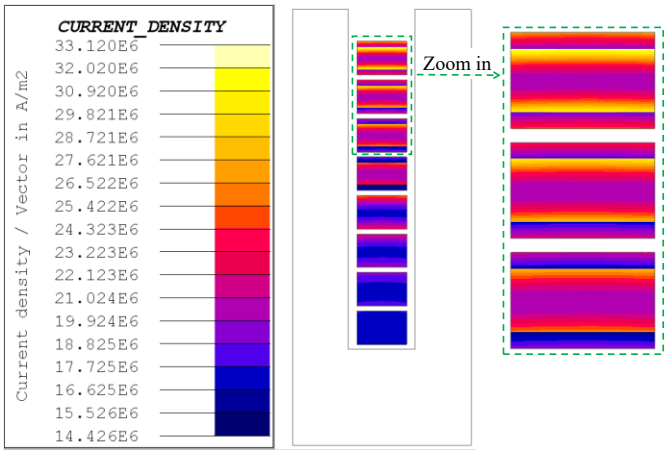

Fig. 5. Peak value of current density map of hybrid 3-layered windings at 500 Hz at 80 A RMS of the excitation current.

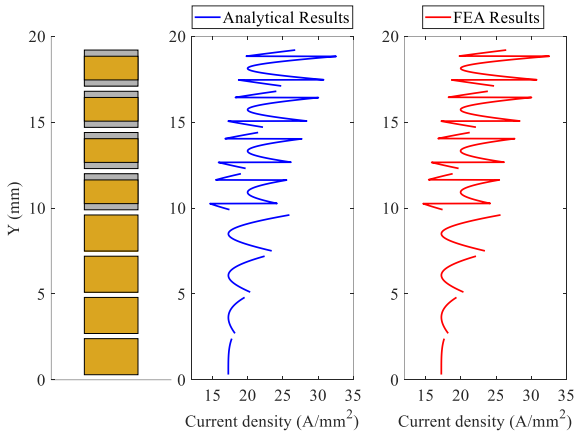

Fig. 6. Peak value of current density of Scheme C at 500 Hz.

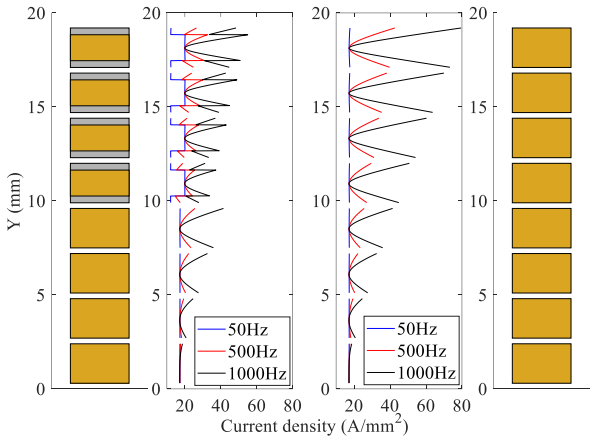

Fig. 7. Comparison of peak value of current density between Scheme C and Scheme A at different frequencies.

C. Effect of the Aluminium Layer Thickness

By changing the aluminium layer thickness h_1, the total winding loss at different frequencies can be plotted as shown in Fig. 8. A thinner aluminium layer, and consequently a thicker central copper conductor, provides superior performance in the lower frequency range. As for the reference of frequency 500 Hz, the total winding losses with layer thickness is plotted in Fig. 9. The minimum loss occurs at a thickness of 0.36 mm. Since the total conductor height is fixed at 2.10 mm, reducing the aluminium layer thickness below 0.36 mm increases the proportion of copper in the conductor. In this range, the aluminium layer becomes too thin to effectively mitigate AC losses, while the larger copper area facilitates stronger eddy currents, resulting in higher losses. Conversely, increasing the aluminium layer thickness above 0.36 mm raises the DC resistance due to the lower conductivity of aluminium, which also leads to higher losses. Fig. 9 highlights that, at a given frequency (e.g., 500 Hz), there is an optimal aluminium layer thickness that balances the AC loss reduction provided by the low-conductivity material and the DC loss minimization offered by copper's high conductivity, achieving the lowest total winding loss.

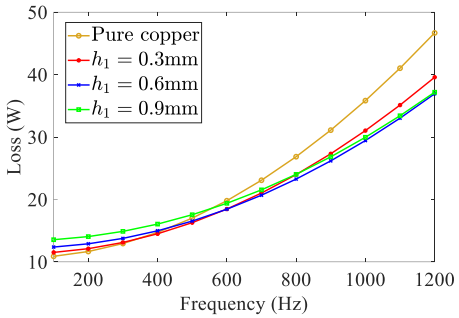

Fig. 8. Total winding loss comparison of different h_1.

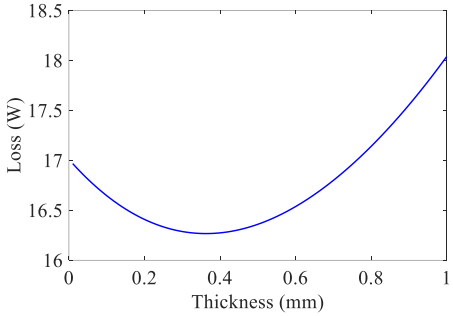

Fig. 9. Total winding loss with different aluminium layer thickness at 500 Hz.

IV. Machine Level Study

The previous sections explored conductor behaviour and losses at a slot level with a frequency domain model. Whereas this provided some useful data for exploring the underlying behaviour, it is the behaviour of a conductor arrangement within a representative electrical machine with multiple sources of time-varying magnetic fields that ultimately determines the benefits or otherwise of hybrid windings. This section presents a time-domain machine level study on a 53 kW, 48-slot, 8-pole machine designed for HEVs (Prius 2017). The 53 kW rating is achieved at a base speed of 3100 rpm which corresponds to a rated torque of 163 Nm [28]. A cross-section of this machine is shown in Fig. 10. This machine has 8 conductors per slot with the same dimensions as detailed in Section II. The rated current of this machine at rated torque is 180 A RMS [29]. Electric circuit-coupled, time-stepped, non-linear and two-dimensional finite element simulation were performed over one fundamental electrical cycle and the losses results were averaged over an electrical cycle.

The total winding losses were extracted from FEA and are summarized in Fig. 11 for 9 specific operating points. At low speeds (e.g., 4000 rpm), the hybrid winding design results in higher losses due to increased DC resistance from the inclusion of low-conductivity materials. However, at 8000 rpm, the hybrid winding shows its advantage over the pure copper winding with a ~5% reduction. This benefit becomes even more significant at higher speeds, reaching a ~10% reduction at 12,000 rpm.

It is interesting to compare the full machine level predictions of winding loss with the predictions from scaling the single slot frequency domain model. Taking the example operating point of 40 A RMS at 4000 rpm, then the losses predicted for the hybrid winding by the full machine model is 156 W while the corresponding single slot valued scaled by the number of slots is 154 W, which results in an underestimate by the single-slot model of 1.1%. Repeating this comparison at the opposite end of the operating range, i.e. 120 A RMS at 12,000 rpm results in the single slot model underestimating the loss compared to the machine level model by 9%. This illustrates that total winding losses of this particular machine can be calculated to a reasonable working accuracy from a single slot model, which in turn tends to suggest that the time varying flux density in the slot is dominated by the self-flux in the slot rather than incident from the rotor permanent magnets and mutual flux due to adjacent slots.

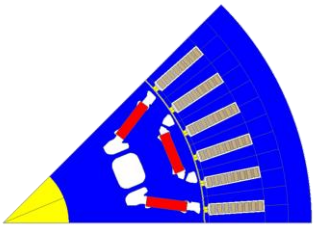

Fig. 10. 48-slot, 8-pole permanent magnet machine.

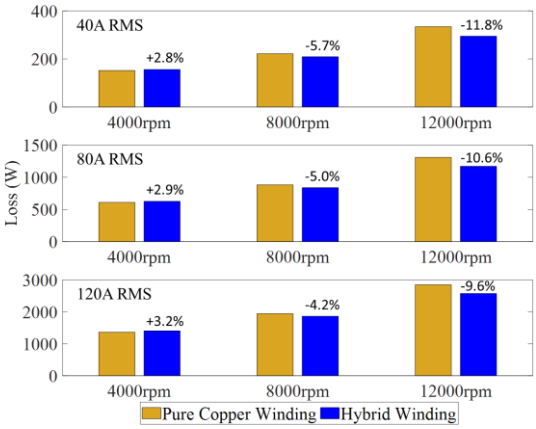

Fig. 11. Total winding losses at 9 different operating points.

While the hybrid conductor does exhibit a higher DC resistance compared to pure copper, its total effective resistance becomes lower in medium-to-high frequency ranges due to mitigated skin and proximity effects. Crucially, since the total magnetomotive force is maintained identical across all conductor types in our comparative study, the mean torque output remains unaffected. The hybrid conductor's layered structure does not alter the winding function, so the back-EMF and flux linkage remains unaffected. While DC losses increase slightly at low speeds, the significant AC loss reduction at high speeds improves overall efficiency at high speeds, which can be turned to get the optimal performance considering the wide operating range of traction motors.

V. Discussion on Materials and Manufacturing

Previous sections analysed the AC loss reduction of the hybrid 3-layer conductor from an electromagnetic point of view. The material of the outer layers does not necessarily have to be aluminium. As long as the selected material has lower

conductivity than copper, the proposed concept is capable of AC loss reduction with proper design.

In practice, joining two different metals presents some potential problems that need to be carefully considered, such as electrostatic corrosion, the possibility of fusion at the boundaries, the feasibility of welding for winding connections, and oxidation. This section will review some possible selections of materials and potential manufacturing processes.

A. Conductivity of the Outer Layer Material

Electrical conductivity is the key parameter that needs to be considered when selecting the conductor materials that make up the overall winding. An evaluation of material conductivity effects from the electromagnetic point of view is provided. Fig. 13 shows the total winding loss of single slot model of different material conductivities (in per unit value with respect the copper conductivity) and different layer thicknesses. For example, aluminium is close to 0.6 p.u. compared to copper conductivity, as indicated by the red columns in Fig. 12. As electrical conductivity decreases, the optimal winding loss can be reduced, but with a narrowed window for layer thickness selection and the optimal thickness becoming thinner.

For the purpose of demonstration, a readily available commercial brass sample was used. This has a composition of ~59% copper and ~41% zinc with an electrical conductivity of 1.35×10^7 S/m, which corresponds to 23% of IACS. By using brass instead of aluminium for the outer layers, the optimal thickness of the brass layer at 500 Hz is 0.31 mm, resulting in a total winding loss of 15.86 W, which is 2.5% lower than the best performance achievable with an aluminium layer. However, this compromises the performance in the DC to low frequency range, as shown in Fig. 13.

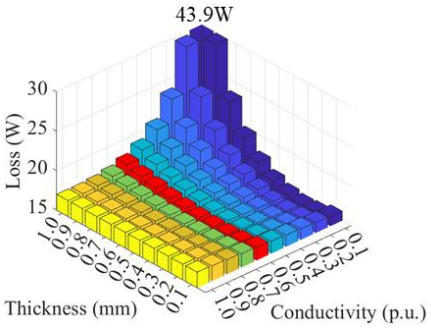

Fig. 12. Total winding loss of different conductivity and layer thickness at 500 Hz.

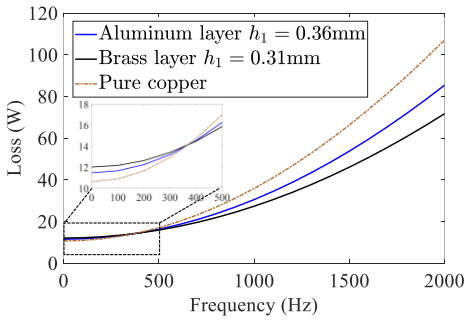

Fig. 13. Total winding loss of aluminium layer and brass layer conductors.

B. Copper and Aluminium

Copper clad aluminium (CCA) wire has attracted attention for applications, such as wireless power transfer [30] due its combination of low-cost, reduced weight, and lower loss caused by proximity effects at high-frequency. A technology for producing copper-aluminium-copper layered composites by explosion welding was presented in [31]. Both these examples demonstrate that cladding copper with aluminium is feasible. However, when different metals come into contact, Intermetallic Compounds (IMCs) can form at the interface between the materials. Under various conditions, IMCs may exhibit very complicated characteristics and composition. By way of example, the effect of moisture and temperature on Al-Cu interfacial strength was studied in [32].

C. Additive Manufacturing

Additive manufacturing, commonly known as 3D printing, enables the fabrication of objects layer by layer based on their digital design data.

As demonstrated in [23, 24], the effective conductivity of a metal could be controlled by controlling the density, as-built orientations, and post-thermal treatment during the additive manufacturing process. This technique can be employed to manufacture the hybrid 3-layer winding design with one more degree of freedom of material properties.

When it comes to printing with two different metals, several techniques are available, each with its advantages and applications as discussed in [33-36]. These additive manufacturing techniques offer the flexibility to print with two different metals simultaneously or sequentially, allowing for the fabrication of complex parts with customized material compositions and properties.

D. Brass and Laser Welding

There are several methods for welding copper and its alloys such as brass, including Gas-Tungsten Arc Welding (GTAW), Gas-Metal Arc Welding (GAA), Plasma Arc Welding (PAW), Electron Beam Welding (EBW), and Laser Beam Welding (LBW) [37, 38]. Reference [39] shows that laser welding is an effective method for joining copper and brass materials with high thermal conductivities due to its ability to provide localized heating and minimal distortion. This method has been applied to manufacturing the conductor samples and presented in Section VI.

VI. Experiment Validation

Following the concept shown in Fig. 2, one U shaped conductor sample has been manufactured using commercial copper (94% IACS) and brass (23% IACS). The overall conductor has a cross-section of 5.2 mm (width) × 3.4 mm (height) and active length of 300 mm in the straight section. The straight section comprised of two 0.8 mm thick brass strips either side of a 1.8 mm thick region of copper. The conducting layers were joined using laser welding on the exposed edges. For the purpose of comparison, a plain copper U-shaped conductor with the same dimensions was also made, as shown in Fig. 14.

At room temperature, the measured DC resistance of the U-shaped hybrid conductor R_{DC-Hyb} is 1.27 mΩ, while that of the corresponding copper only conductor R_{DC-Cu} is 0.93 mΩ. Subsequently, the U-shaped hybrid conductor was placed in a two-slot motorette made of M250-35A laminated sheets with a stack length of 300 mm. A cross-section of the slot geometry as well as the test set-up is shown in Fig. 15. The sixth turn which consists of the U-shaped hybrid or copper only conductor is located in the position nearest the slot-opening. A 5-turn coil of the same cross-section made with AlSi10Mg by additive manufacturing was positioned at the slot bottom, with the U-shaped conductors of Fig. 14 successively serving as the sixth series connected turn. The resistance was measured using a Hioki IM3570 impedance analyzer as shown in Fig. 16.

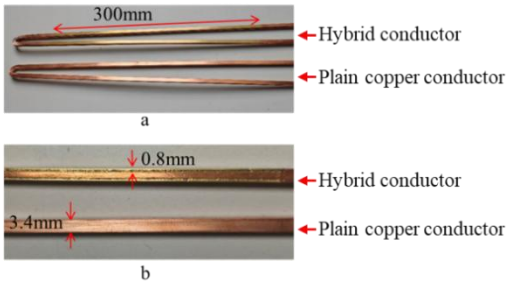

Fig. 14. Test samples. (a) Two single turn U-shaped conductors. (b) Sideview of the 3-layer structure.

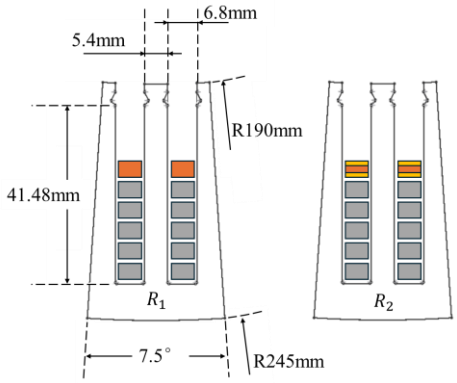

Fig. 15. Cross-section of the slot geometry.

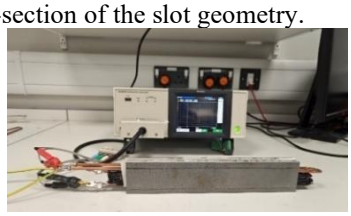

Fig. 16. Test with Hioki IM3570 impedance analyzer.

To eliminate the effect of iron loss and AC losses in the 5-turn section of the coil, a differential method was employed as follows:

The impedance analyzer was set in constant current mode to supply a constant 50 mA RMS current. The first measurement was taken with the plain copper U shaped conductor as the sixth turn, denoted as R_1. Subsequently, the plain U-shaped copper conductor was replaced by a brass-copper hybrid U-shaped conductor of the same dimensions as the sixth turn, and the second measurement was taken, denoted as R_2. Since the current remained at 50 mA in both tests, the total MMF in the slot remains the same and, to a reasonable approximation, the iron loss can be assumed to remain unchanged. Hence, the difference between the two tests, $R_2 - R_1$, represents the effect of the hybrid conductor on the AC loss.

Fig. 17 shows the measured resistance difference, indicating that the hybrid conductor exhibits a lower resistance compared to the plain copper conductor once the frequency exceeds 300 Hz. The DC resistance of the single-turn copper conductor R_{DC-Cu} is also plotted (as the dash-dotted line) to provide a reference for the scale of resistance reduction.

Fig. 18 compares the experimentally measured results with the FEA-predicted results over a frequency range extending to 5000 Hz. The discrepancy between the experimental results and FEA predictions could be attributed to the joint resistance R_j in the end part, as illustrated in Fig. 19. Since the joint resistance is not included in the simulation model, the experimentally measured resistance is higher than the FEA-predicted resistance.

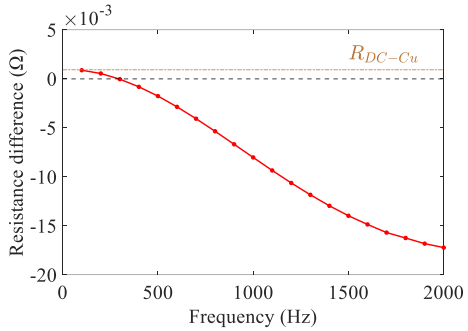

Fig. 17. Measured difference of resistance of hybrid conductor and copper conductor up to 2000 Hz.

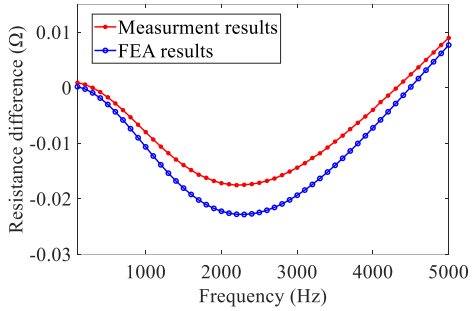

Fig. 18. Difference of resistance of hybrid conductor and copper conductor up to 5000 Hz.

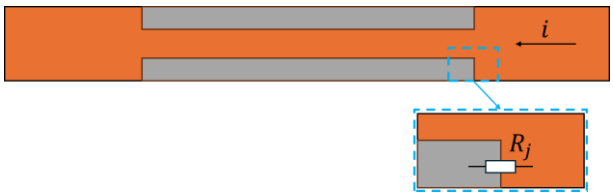

Fig. 19. Illustration of joint resistance in the end part.

Despite the joint resistance contributing additional losses in the hybrid conductor, it still demonstrates advantages over the plain copper conductor across a wide frequency range. A comparison between the hybrid conductor and the plain copper conductor in terms of AC resistance as the sixth turn is shown

in Fig. 20. Since the experimental setup does not directly measure the AC resistance of the conductor, the AC resistance for the plain copper conductor was obtained from FEA, and the difference from experimental measurements was added to estimate the AC resistance of the hybrid conductor. Fig. 20 illustrates that within the frequency range of 300 Hz to 4300 Hz, the hybrid conductor consistently exhibits lower AC resistance compared to the plain copper conductor. Notably, at 2200 Hz, the measured results reveal the most substantial difference, with a reduction of 17.6 mΩ, representing a significant 29.4% decrease relative to the AC resistance of the copper conductor at that frequency.

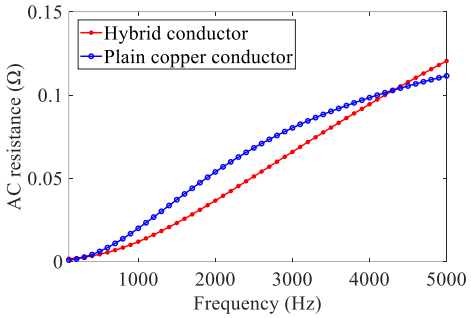

Fig. 20. Comparison of AC resistance between the hybrid conductor and the plain copper conductor.

VII. Conclusion

This paper presents a hybrid bar conductor design that combines the low DC resistance of copper with the reduced AC losses of low-conductivity materials (e.g., aluminium or brass). By integrating an outer layer of lower conductivity, the proposed design mitigates skin and proximity effects at high frequencies without altering the original winding layout. An analytical model of the hybrid 3-layered winding is proposed for current density and total loss prediction, validated by the corresponding FEA results. Experimental tests with brass-copper hybrid conductors confirm the effectiveness of the design. The proposed hybrid conductor provides another set of parameters that a designer can use to tune performance, and it can be considered as an add-on feature to improve existing copper winding designs. Future work will explore thermal effects, PWM-induced losses, multi-objective optimization for enhanced power density, and machine level loss measurements.

References

[1] Y. Zhao, D. Li, T. Pei, and R. Qu, "Overview of the rectangular wire windings AC electrical machine," CES Transactions on Electrical Machines and Systems, vol. 3, no. 2, pp. 160-169, 2019.
[2] A. Arzillo et al., "Challenges and Future opportunities of Hairpin Technologies," 2020: IEEE,
[3] S. Singh, R. Krüger, and M. Doppelbauer, "Comparison of Optimized Hairpin and Pull-in Winding High-Speed Electrically Excited Synchronous Machines for Traction Applications," presented at the 2023 13th International Electric Drives Production Conference (EDPC), 2023
[4] A. Arzillo et al., "Challenges and Future Opportunities of Hairpin Technologies," (in English), Proc Ieee Int Symp, pp. 277-282, 2020.
[5] M. S. Islam, I. Husain, A. Ahmed, and A. Sathyan, "Asymmetric Bar Winding for High-Speed Traction Electric Machines," IEEE Transactions on Transportation Electrification, vol. 6, no. 1, pp. 3-15, 2020.
[6] I. L. Acevedo, M. Osama, D. Filusch, and H.-G. Herzog, "Design of Shaped Electric Machine Windings to Reduce Ohmic Losses," presented at the 2023 13th International Electric Drives Production Conference (EDPC), 2023
[7] Y. Yamada and H. Sugimoto, "Pentagonal and Rectangular Coils for AC Loss Reduction in Electric Machines," presented at the 2023 IEEE International Electric Machines & Drives Conference (IEMDC), 2023
[8] F. Momen, K. Rahman, and Y. Son, "Electrical Propulsion System Design of Chevrolet Bolt Battery Electric Vehicle," IEEE Transactions on Industry Applications, vol. 55, no. 1, pp. 376-384, 2019.
[9] E. Preci et al., "Segmented Hairpin Topology for Reduced Losses at High-Frequency Operations," IEEE Transactions on Transportation Electrification, vol. 8, no. 1, pp. 688-698, 2022.
[10] M. Pastura, R. Notari, S. Nuzzo, D. Barater, and G. Franceschini, "AC Losses Analysis and Design Guidelines for Hairpin Windings With Segmented Conductors," IEEE Transactions on Transportation Electrification, vol. 10, no. 1, pp. 33-41, 2024.
[11] T. Yu, Y. Gai, and J. Guo, "AC Copper Loss Analysis of Hairpin Windings for Permanent Magnet Synchronous Motors Considering Eddy Current Effects," presented at the 2023 IEEE 6th Student Conference on Electric Machines and Systems (SCEMS), 2023
[12] M. Aoyama and J. Deng, "Visualization and quantitative evaluation of eddy current loss in bar-wound type permanent magnet synchronous motor for mild-hybrid vehicles," CES Transactions on Electrical Machines and Systems, vol. 3, no. 3, pp. 269-278, 2019.
[13] K. Zhang, Y. Liang, P. Yang, and D. Wang, "AC Loss Calculation of Integral Transposed Winding in PM Motor for Electric Vehicles," IEEE Transactions on Transportation Electrification, pp. 1-1, 2024.
[14] X. Ju, Y. Cheng, B. Du, M. Yang, D. Yang, and S. Cui, "AC Loss Analysis and Measurement of a Hybrid Transposed Hairpin Winding for EV Traction Machines," IEEE Transactions on Industrial Electronics, vol. 70, no. 4, pp. 3525-3536, 2023.
[15] H. Fang, Q. Chen, X. Wan, and A. Li, "Design and Optimization of High Efficiency Flat wire Motor for Electric Vehicle," presented at the 2023 China Automation Congress (CAC), 2023
[16] Y. Sun, X. Chen, W. Zhu, and G. W. Jewell, "An Investigation of Substituting Copper with Aluminum Conductors in a High Power, Medium Speed SPM Machine," presented at the 2023 IEEE Transportation Electrification Conference and Expo, Asia-Pacific (ITEC Asia-Pacific), 2023
[17] S. Yangyu and G. W. Jewell, "An investigation into the influence of stator tooth and conductor geometry on AC winding losses in a 365kW permanent magnet machine equipped with rectangular bar conductors," 2022.
[18] H. Sugimoto, Y. Yamada, and K. Imae, "Analysis of Winding AC Loss in a Permanent Magnet Synchronous Machine With High Slot Fill Aluminum Winding," (in English), 2022 International Power Electronics Conference (Ipec-Himeji 2022- Ecce Asia), pp. 2741-2745, 2022.
[19] P. Mellor, N. Simpson, and D. North, "Computational efficient design framework for low AC loss, 3D printed windings," presented at the 2023 IEEE Energy Conversion Congress and Exposition (ECCE), 2023
[20] N. Simpson, D. North, P. Munagala, H. Felton, P. Mellor, and A. Helm, "Litzpins: Hybrid Solid-Transposed Hairpin Conductors Enabled By Additive Manufacturing," presented at the 2023 IEEE International Electric Machines & Drives Conference (IEMDC), 2023
[21] R. Notari, S. Nuzzo, F. Savi, S. Defanti, and D. Barater, "An Asymmetrical Additively Manufactured Hairpin Winding for increased efficiency and sustainability," IEEE Transactions on Transportation Electrification, pp. 1-1, 2024.
[22] R. P. Wojda and P. R. Kandula, "Additively Manufactured Copper Windings with Hilbert Structure," presented at the 2023 IEEE Energy Conversion Congress and Exposition (ECCE), 2023
[23] N. Simpson, S. P. Munagala, A. Catania, F. Derguti, and P. H. Mellor, "Functionally Graded Electrical Windings Enabled by Additive Manufacturing," presented at the 2022 International Conference on Electrical Machines (ICEM), 2022
[24] F. Wu, A. M. El-Refaie, and A. Al-Qarni, "Minimization of Winding AC Losses Using Inhomogeneous Electrical Conductivity Enabled by Additive Manufacturing," IEEE Transactions on Industry Applications, vol. 58, no. 3, pp. 3447-3458, 2022.
[25] C. Liu, V. Cecchi, C. Liu, and S. Kamel, "Analysis of AC Resistance in Non-Ferrous Bimetallic Solid Conductors," (in English), North Amer Pow Symp, 2015.

[26] D. Lin, C. Lu, N. Chen, and P. Zhou, "An Efficient Method for Litz-Wire AC Loss Computation in Transient Finite Element Analysis," IEEE Transactions on Magnetics, vol. 58, no. 5, pp. 1-10, 2022.
[27] Y. Wang, J. Pries, K. Zhou, H. Hofmann, and D. Rizzo, "Computationally Efficient AC Resistance Model for Stator Winding With Rectangular Conductors," IEEE Transactions on Magnetics, vol. 56, no. 4, pp. 1-9, 2020.
[28] A. Krings and C. Monissen, "Review and Trends in Electric Traction Motors for Battery Electric and Hybrid Vehicles," 2020: IEEE,
[29] J. T. Shi, R. P. Deodhar, C. Umemura, and A. Pride, "Comprehensive Study of Variable Flux Memory Machines with Symmetrical Series Hybrid Permanent Magnets in Rotor Pole," 2020: IEEE,
[30] C. K. N. Guan, T. Shinmoto and K. Yashiro, "AC resistance of copper clad aluminum wires," presented at the 2012 International Symposium on Antennas and Propagation (ISAP), Nagoya, Japan, 2012
[31] V. Dragobetskii, A. Shapoval, E. Naumova, S. Shlyk, D. Mospan, and V. Sikulskiy, "The Technology of Production of a Copper - Aluminum - Copper Composite to Produce Current Lead Buses of the High - Voltage Plants," (in English), 2017 International Conference on Modern Electrical and Energy Systems (Mees), pp. 400-403, 2017.
[32] H. Teng, H. L. Zhang, H. B. Yang, M. Zhou, and A. C. Tsui, "Effect of Moisture and Temperature on Al-Cu Interfacial Strength," (in English), 2008 International Conference on Electronic Packaging Technology & High Density Packaging, Vols 1 and 2, pp. 688-691, 2008.
[33] X. Zhang et al., "Additive manufacturing of copper – H13 tool steel bi-metallic structures via Ni-based multi-interlayer," Additive Manufacturing, vol. 36, 2020.
[34] H. Wu et al., "Bonding behavior of Bi-metal-deposits produced by hybrid cold spray additive manufacturing," Journal of Materials Processing Technology, vol. 299, 2022.
[35] F. Marefat, J. De Pauw, A. Kapil, N. Chernovol, P. Van Rymenant, and A. Sharma, "Design strategies for bi-metallic additive manufacturing in the context of wire and arc directed energy deposition," Materials & Design, vol. 215, 2022.
[36] A. Bandyopadhyay, Y. Zhang, and B. Onuike, "Additive manufacturing of bimetallic structures," Virtual and Physical Prototyping, vol. 17, no. 2, pp. 256-294, 2022.
[37] L. Zhou, W. L. Zhou, J. C. Feng, W. X. He, Y. X. Huang, and S. S. Dong, "Effect of rotation speed on the microstructure and mechanical properties of dissimilar friction stir-welded copper/brass metals," The International Journal of Advanced Manufacturing Technology, 2015.
[38] F. Gharavi, I. Ebrahimzadeh, K. Amini, and P. Darya, "Evaluation of the microstructure and mechanical properties of friction stir-welded copper/brass dissimilar joints," Materials Research Express, vol. 5, no. 7, p. 076517, 2018.
[39] P. Dong and R. Xiao, "Laser welding of lap joint between copper and brass," in International Laser Safety Conference, 2009: AIP Publishing, pp. 203-207.